Monte-Carlo Studies for The MAGIC Telescope Project

J. C. González[1,2], R. Mirzoyan[1*], V. Fonseca[2] and E. Lorenz[1]

[1]*Max-Planck-Institut für Physik, Föhringer Ring 6, 80805 München, Germany.*
[2]*Dpto. Física Atómica Molecular y Nuclear. Fac. CC. Físicas. U.C.M. 28040 Madrid, Spain.*

Abstract

The energy range 10–300 GeV in cosmic gamma rays is not yet investigated due to the lack of detectors in this domain. The MAGIC Telescope project is dedicated to gamma ray astronomy above the lower threshold 10–30 GeV and will provide measurements with very high sensitivity up to $\sim$50–100 TeV. Here we present the main results of Monte Carlo studies performed for the 17 m diameter MAGIC Telescope.

1. Introduction

We have studied the main characteristics of the MAGIC Telescope by using the version 4.52 of CORSIKA air shower simulation program (Knapp and Heck, 1995). The simulations include the atmospheric absorption and scattering processes as the Rayleigh scattering, the Mie scattering and the aerosol and Ozone absorption (Gaisser, 1990). The effect of the Earth magnetic field was also included. We used the 300–600 nm wavelength range to simulate Cherenkov light from air showers, saving the direction, relative time of arrival and the wavelength of every photon hitting the reflector.

In order to investigate the realistic characteristics of MAGIC and to take into account the optical aberrations introduced by its reflector we developed two independent optical ray tracing programs. These were confronted and one of them was included in our Monte Carlo simulations. MAGIC will have a tessellated reflector of 17 m diameter, consisting of 932 square mirrors (+40 triangular ones) of spherical curvature, measuring $50\times 50\,cm^2$ each. The curvature of the reflector has been chosen to be parabolic in order to provide high angular resolution in the central part of the field of view. The parabolic reflector also provides the minimum time dispersion in the focal plane for collected light from a plane front of a parallel beam. The radius of curvature of the mirror tiles varies between 34–36 m depending on their distance from the optical axis of the reflector. We defined the exact position and orientation of each single mirror element in simulations, as well as we took into account the planned 5 mm gaps between neighbouring ones. Furthermore, we assume a flat 85% reflectivity for mirrors.

The Cherenkov photons from showers were traced through the atmosphere and the coordinates of reflected photons in the focal plane were obtained from the ray tracing program. In this way we simulated realistic aberrations for the tessellated reflector of MAGIC. Ray tracings showed that 50% of all photons, impinging on the reflector of MAGIC from a point source of light at infinity, will be collected in spots of diameters of 0.06°, 0.11° and 0.15° in the focal plane for the beam incident angles of 0.5°, 1.0° and 1.5° correspondingly. The detailed ray tracing will be presented in (Barrio et al.).

Fig.1 shows the evolution of the shape of Cherenkov spectrum emitted by 50 GeV gamma showers after the application of different steps in simulations. The curve 1 (the top one) shows

---

*On leave from Yerevan Physics Institute, Yerevan, Armenia.

Cherenkov spectrum emitted by shower particles in the atmosphere. The curve 2 shows the resulting spectrum after application of the atmospheric attenuation processes. The curve 3 shows change of the spectrum due to lost photons in the inter-mirror gaps. The curves 4 and 5 show the spectra after applying the mirror reflectivity and the photon collection efficiency of the focal plane camera. The curve 6 shows the spectrum after the application of a flat 45% QE of *enhanced sensitivity hybrid photomultipliers* (HPMT) (see section 3.).

2. Generation of the MC library

We assumed in calculations an observation altitude of $2200\,m$ a.s.l. We have simulated gamma ray showers in the energy range $5\,GeV$–$10\,TeV$ and in the impact parameter range 0–$350\,m$. Presently we have simulated showers only for zenith angle 0°. The number of generated gamma ray events is few hundreds per energy bin for $E_\gamma \geq 500\,GeV$, several thousands for energy bins between 80–$250\,GeV$ and few tens of thousands per bin below $80\,GeV$. Taking into account the high trigger efficiency for gammas, this provides a reasonable amount of data for Monte Carlo studies.

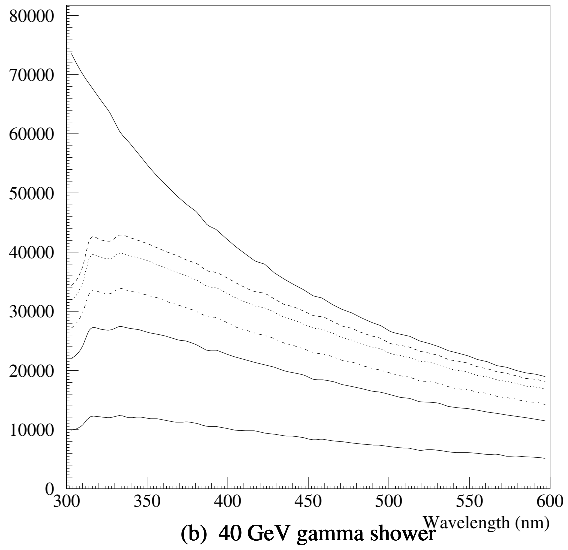

Fig. 1: The evolution of Cherenkov spectrum (the Y axis is in arbitrary units) of $50\,GeV$ gammas after application of different steps in simulations (see the text for details)

For the hadronic background we assume that it is entirely formed by protons. In reality, the protons are ∼43% in the chemical composition at $1\,TeV$ (Wiebel, 1994). However, the heavier components in cosmic rays contribute only ∼25–30% into the total rate measured by Cherenkov telescopes. Therefore the consideration of only a proton-like background should be a conservative approach for studying the achievable gamma/hadron separation.

The proton showers were simulated within an angular acceptance of ±4° around zenith and for the impact parameter range 0–$350\,m$. The number of simulated proton showers is several hundreds per energy bin for $E_p \geq 2\,TeV$, few thousands for energy bins $E_p \geq 100\,GeV$ and several tenths of thousands for energies below $100\,GeV$. The latter is necessary because the protons are already very strongly rejected at the trigger level. For example, the average trigger efficiency for protons of $60\,GeV$ is ∼0.25%, it drops down to the level of 0.15% for $40\,GeV$ and it is only 0.025% for $30\,GeV$, i.e. only one out of 4000 produces enough light to initiate a trigger in a HPMT high QE camera..

3. The Camera

We have simulated three types of focal plane imaging cameras. As a first type we used a 5° diameter camera with imaginary light sensors of 100% QE and of infinitely small pixel size i.e. each photon hitting the camera was detected. In both 3.5° diameter cameras of the second and of the third type a pixel size of 0.1° was used. The light sensors of the second camera were assumed to be HPMTs with GaAsP photocathode, providing $\sim 45\%$ QE in the whole 300–600 nm range. The third camera pixels were assumed to be classical photomultipliers (PMTs). In the latter case we took the QE dependence on the wavelength from the measurement of 19 mm diameter EMI-9083A bialkali PMTs (Mirzoyan, Fernandez et al.). When a photon of a given wavelength, different from the measured ones hit the PMT, the value of QE was taken by a third order approximation between the closest measured wavelengths. For MAGIC we plan to use 397 pixels of $0.1°$ size in the camera central part, which provides a diameter of $\sim 2.3°$. The outer part of the camera till the radius $\sim 1.75°$ will probably have 1.5–2 times larger pixel size, but for simplicity we used the same pixel size of $0.1°$ in simulations for the entire camera. We assumed 90% light collection efficiency for the light guides which are supposed to be attached to the light sensors. Also we assumed 90% ph.e. collection efficiency for both the second and the third type cameras. Fig.2 shows an image of a 60 GeV gamma shower prior to any cuts, seen by the enhanced QE HPMTs camera.

4. The Trigger

MAGIC will have a very high photon sensitivity due to the large surface area of its reflector. This will result in a very low threshold and correspondingly in a high trigger rate. The excessive rate of isotropic background showers can force one to use rather sophisticated and expensive data acquisition system. On the other hand the rate of the isotropic backgrounds is proportional to the solid angle of the part of the camera which is set into the trigger. We optimised the trigger area providing high trigger rate for gammas and simultaneously low rate from different backgrounds.

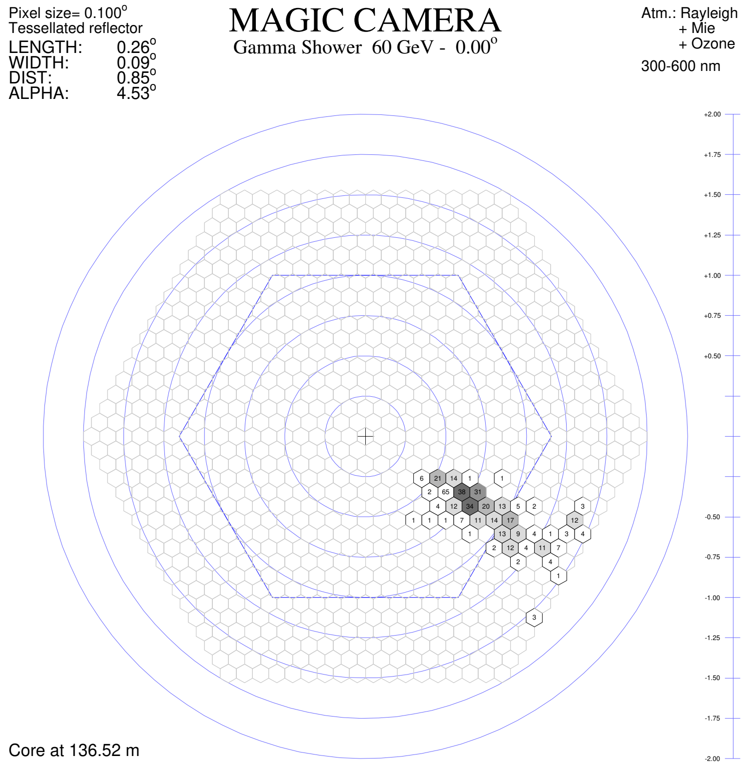

Fig. 2: An image of a 60 GeV gamma prior to any cuts, seen by the enhanced QE HPMT camera.

The sub-100 GeV gamma showers develop higher up in the atmosphere compared to TeV ones and therefore a telescope "sees" them at smaller angles i.e. their images are closer to the camera centre. This means that for sub-100 GeV gammas one needs in principle an effectively smaller camera diameter compared to observations in the TeV energy range.

We found that the camera trigger radius of $0.8°$ is a good compromise for MAGIC. When the trigger radius of the camera is limited to $\leq 0.8°$, together with sub-100 GeV showers also those above 100 GeV, in spite of the fact that their centroids can be at distances $\geq 0.8°$ for large impact parameters, will readily trigger the camera. This is the result of the high photon sensitivity of the telescope, its low trigger threshold per pixel and the higher light intensity along the images of high energy showers compared to low energy ones.

The aim of simulating background showers within a much wider angle of $\pm 4°$ than the trigger radius of $0.8°$ of the camera, is twofold:

- One takes into account triggers due to inclined showers. The axes of these showers are outside the acceptance of the system, but the light coming from them nevertheless can reach the camera. This is possible due to large multiple scattering angles and high transverse momentum of charged particles in hadron showers.

- Also, one takes into account triggers due to Cherenkov light emission of charged single particles in air showers as, for example, from muons. The latter can sometimes have non-negligible angles with respect to the shower axes and though the shower itself can be outside of the camera acceptance, the muon can be in its field of view and Cherenkov light from it can produce a trigger.

The trigger condition "*any 4 neighbour channels in a close pack above the pre-set threshold of 7 ph.e.s*" has been applied both for gammas and protons for both camera options. This rather strong trigger condition allows one to suppress the accidental triggers due to light of night sky (LONS) and after-pulsing (when relevant) and to lower the trigger threshold. It allows one to trigger with high efficiency on gammas and strongly suppresses hadron triggers due to the more diffuse shape of their images. It is well known that sub-100 GeV hadrons produce several times less Cherenkov light than gammas of similar energies (Weekes and Turver, 1977). Therefore, one should expect that this trigger condition will help to trigger readily on sub-100 GeV gammas, while on average hadronic showers with energies above 100 GeV produce sufficient light to pass the trigger threshold. Moreover, due to the diffuse character and the lower light content in proton images and the strong trigger condition they trigger with much less probability. It should be mentioned that due to lower QE of classical PMTs compared to HPMTs, the former integrate less light from LONS and therefore one can apply a weaker trigger condition, say for example, "any 4 neighbour pixels above a threshold of 4 ph.e.s", which will result in a somewhat lower threshold and correspondingly higher trigger rates. Therefore one can consider our results for the PMT camera option, as rather conservative.

5. Muon Arc Triggers

The problem of cosmic ray muon background, triggering Cherenkov telescopes through the so-called muon-rings (see, for example, Vacanti, Fleury et al.,) is not yet fully studied. There is still little accumulated experience in how to handle this problem. As all the muons triggering the telescopes are produced in air showers, it seems that one should not consider two different components, that is, the light coming from the muon and from the shower itself, which can initiate independent triggers. Instead, one should simulate hadron showers for a relatively large acceptance angle

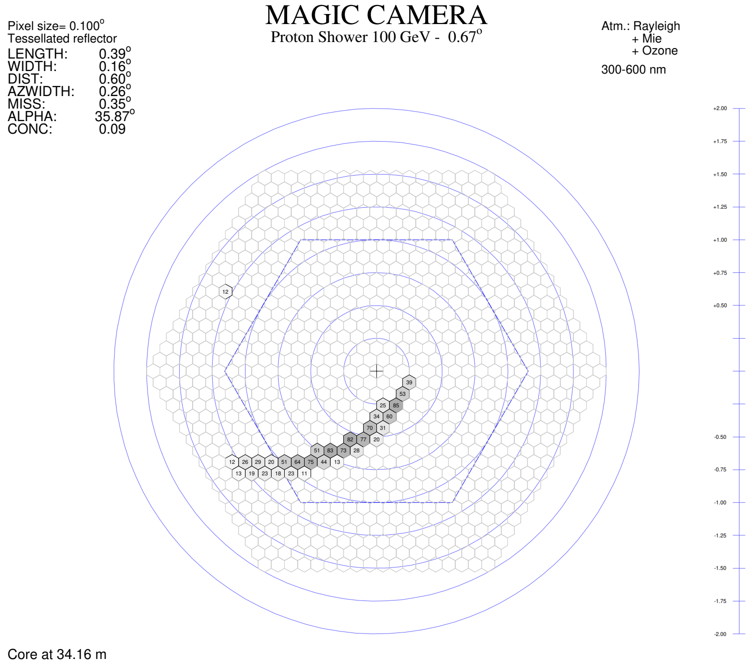

Fig. 3: An image of a muon arc produced in a 100 GeV *proton event.*

and also for very low energies. This has been the strategy in our simulations. On Fig.3 is shown a muon event produced by a $100\,GeV$ proton. One of the characteristic features of muon images is their high charge concentration along the images. Note, that muons from large impact parameters ($\geq 80\,m$) produce images like blobs of very high charge concentration just in a couple of pixels.

6. The Influence of the Light of the Night Sky

We took into account the influence of the background light of the night sky, the intensity of which has been measured at La Palma, at the site of the HEGRA experiment. The LONS intensity I for the narrow angle detector (acceptance angle less that $1°$) in the 300–600 nm range was measured to be $I = (1.7{\pm}0.4){\cdot}10^{12}\,ph/m^2\,s\,sr$ (Mirzoyan and Lorenz, 1994). Taking into account the envisaged $300\,MHz$ flash ADCs (intended to be used for the data acquisition), some other relevant values and using the mentioned LONS intensity, we estimate an average value for LONS contribution of 3 ph.e.s per pixel per measured event for the high QE HPMT camera and 0.5 ph.e.s for the classical PMT camera. In simulations of shower images the poissonian fluctuations of the above mentioned values are added to the genuine charge measured in a given pixel. In the transformation from signal photons to ph.e.s at first the mean number of ph.e.s is determined by using the given QE(λ) and then the final measured charge is determined from the fluctuations in the mean.

7. The Results

Here we present the results of Monte Carlo studies for MAGIC for both types of cameras, and the follow-up analysis. Note that most of the physical parameters calculated and shown here are very strongly energy-dependent. Due to the power low spectra, the calculated values refer mostly to an energy close to the threshold. Therefore, the comparison with similar numbers for different telescopes should be done by taking into account the detector-specific features.

7.1. The Collection Areas

On Figure 4, the effective collection areas for gamma and proton showers after trigger for both camera options are shown. For example, the collection area after trigger amounts to $10^4\,m^2$ already for $10\,GeV$ gamma rays, for $20\,GeV$ gammas it is $\sim 3.5 \times 10^4\,m^2$ and for energies above $80\,GeV$ it reaches the asymptotic value of $\sim 10^5\,m^2$ in the case of the high QE HPMT camera. Note, that the trigger collection area for protons is much smaller than for gammas. For very low energies it is smaller by almost three orders of magnitude.

7.2. The Trigger Efficiency

The trigger efficiency for gamma rays is much higher than for protons. For example, for an impact parameter up to $130\,m$ the $20\,GeV$ gamma showers trigger the telescope with average probability of 45%, while it increases to 70% at $40\,GeV$. The $60\,GeV$ gammas trigger with 90% probability and the $80\,GeV$ gammas trigger with a probability of 95%. Above this energy, the trigger probability reaches the plateau level of almost 100%. Protons trigger with much lower probability. The $30\,GeV$ protons trigger with a probability of only 0.025%, while it reaches the level of 1.4% for $100\,GeV$ showers. The $250\,GeV$ proton showers trigger with a probability of

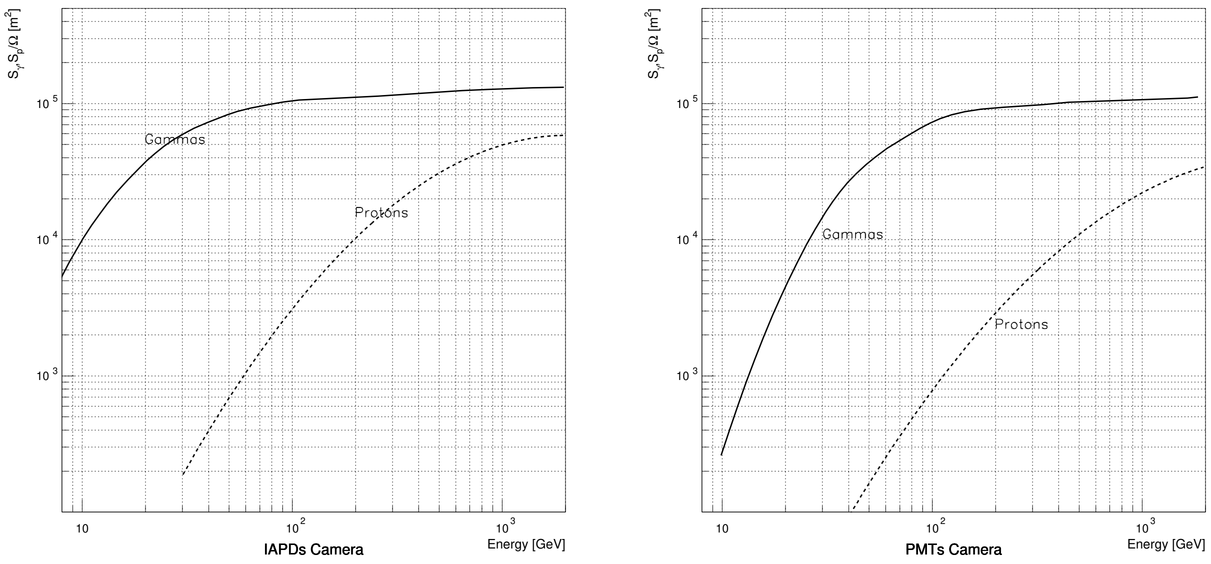

Fig. 4: The effective collection areas for gammas and protons after trigger for 0.8° camera trigger radius for the enhanced QE HPMT (left) and the classical PMT cameras (right).

8%–12%, and 500 GeV proton showers trigger with a probability of 10%–15%. One can see that the application of the "*any* ≥ 4 *neighbours*" trigger condition results in a very strong rejection of proton images, providing already at the trigger level a highly efficient pre-selection of gamma rays.

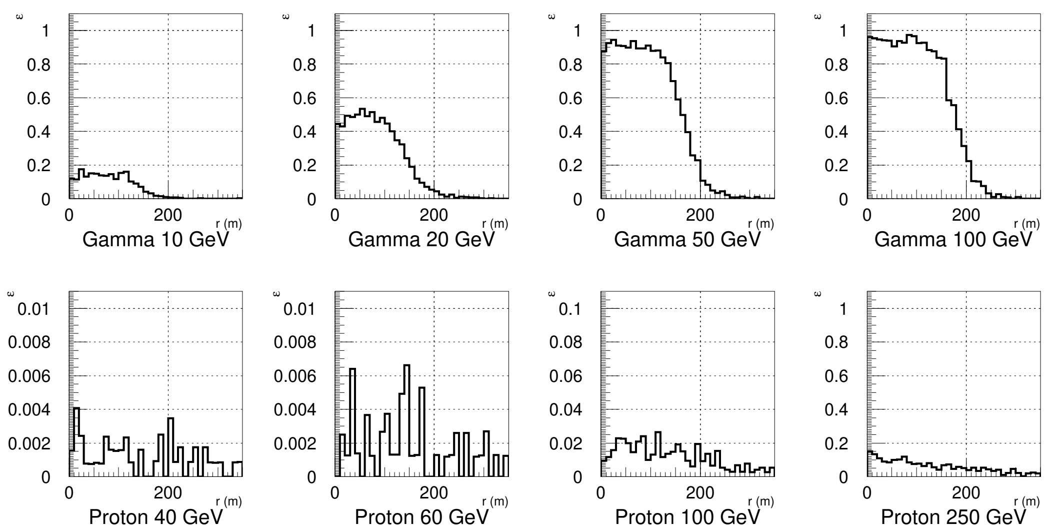

Fig. 5: The trigger Efficiency for gamma and proton showers in the energy range 10 GeV–250 GeV (note the different scales in the histograms for the proton showers).

7.3. The Rates

On Fig.6 the gamma and proton differential rates for MAGIC, simulated for a camera trigger radius of 0.8°, are shown. In this simulations we assumed a gamma-ray emitting point source with an integral flux normalisation of $F_\gamma(E) = 10^{-8}(E/10\,GeV)^{-1.5}\,ph\,cm^{-2}\,s^{-1}$. (with an spectral index $\alpha = -2.5$). One can see that the threshold of the telescope, which is usually defined as the peak of its differential rate for gammas, is at energies somewhat lower than $10\,GeV$, at about $8\,GeV$. By integrating the above shown differential rates we obtained a gamma ray trigger rate of $3.5\,Hz$ and a cosmic ray background (assumed to be all protons) of about 80 Hz (see Figure 7) for the high QE HPMT camera (note again, that this rate includes the rate due to the muon-arcs). This very high signal to noise ratio is first of all due to the high trigger efficiency for gammas and very low efficiency for protons. One can conclude that even a moderate gamma/hadron separation in the imaging analysis will provide a very high sensitivity for the telescope. Also, we estimated a trigger rate of $\sim 8\,Hz$ from cosmic electrons. This isotropic background can be effectively suppressed by using the On/Off measuring mode, the angular resolution of the telescope and the asymmetry of showers. The electron background will slightly degrade the sensitivity of the telescope. On Figure 6 one can see that the threshold of the telescope with the classical PMT camera is around $30\,GeV$.

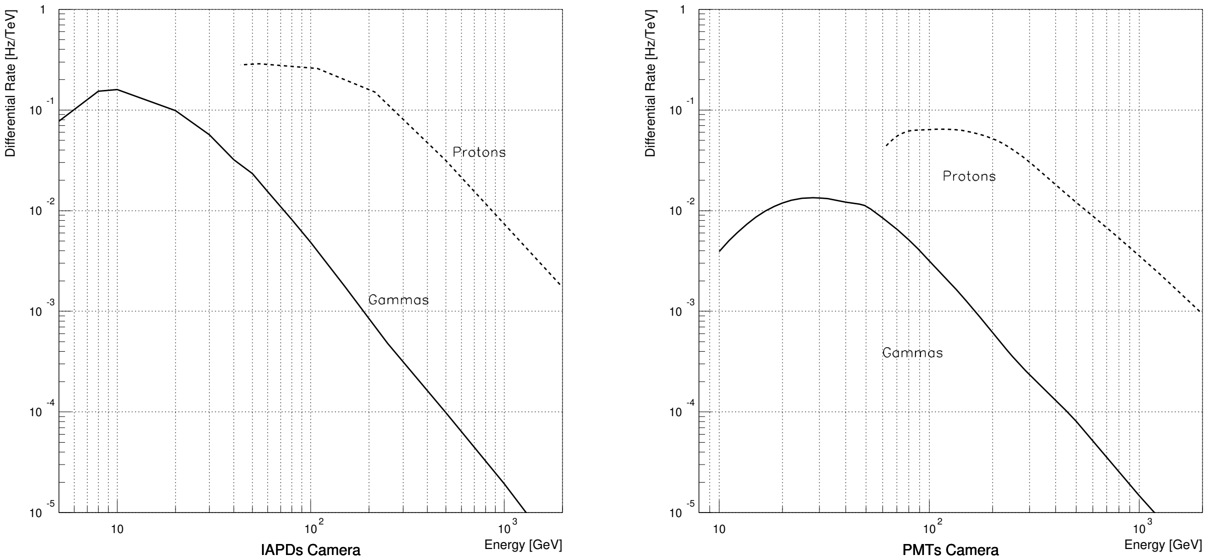

Fig. 6: The simulated differential rates for gammas and protons for 0.8° trigger radius of the camera for the enhanced QE HPMT (left) and the classical PMT cameras (right).

7.4. The Imaging Analysis

We found that at low energies the power of "classical" second moment image analysis technique degrades. Both the shape and the angular parameters of images of showers have broader distributions than at higher energies. The very low energy showers develop higher in the atmosphere where the air density is low and the threshold energy for Cherenkov light production is high. The telescope measures such showers at smaller angles, which means that the images are at shorter distances from the camera centre and they are more round. Due to the mentioned reasons also the fluctuations in images are larger.

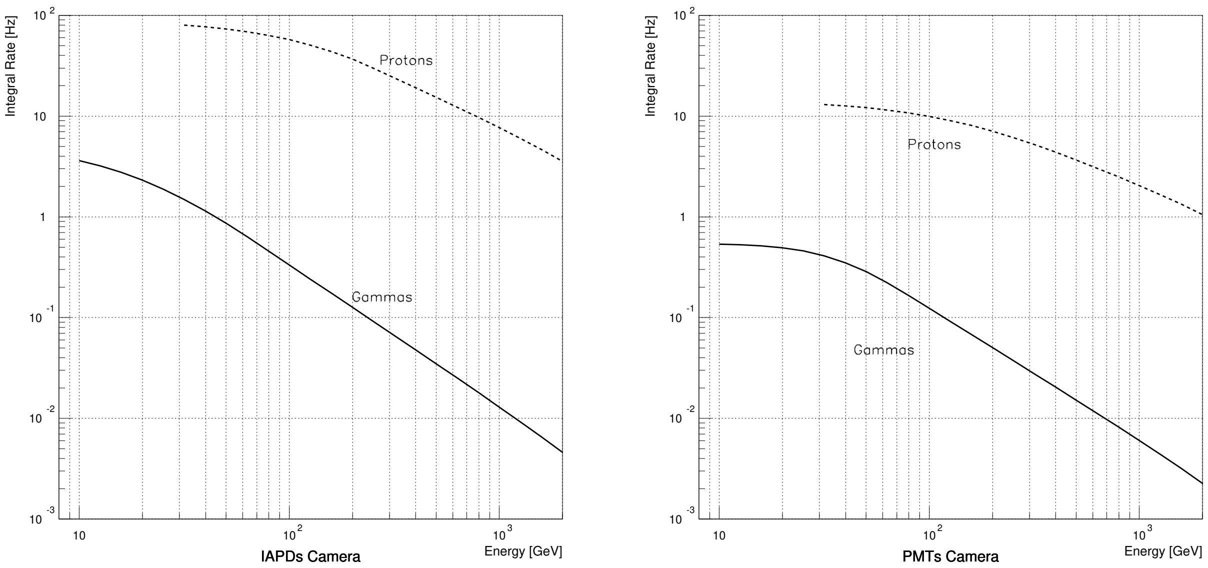

Fig. 7: The integral rates for gammas and protons for 0.8° trigger radius of the camera for the enhanced QE hybrid PMT (left) and the classical PMT cameras (right).

In order to investigate the achievable quality factor Q in software analysis of images, by using generated Monte Carlo events we simulated a gamma spectrum from $10\,GeV$ to $10\,TeV$ with the differential spectral index and spectrum normalisation above mentioned and a background proton spectrum with an index of -2.75. Instead of the image parameter DISTANCE we used a modified parameter MaxDIST (in the camera plane it is the distance between the source position and the interpolated coordinate of maximum amplitude in the image, which should correspond to the angular distance to the shower maximum). We used the range of 0.4°–1.1° for the parameter MaxDIST, which we split into three bins. For each of these bins, after a *Tail-Cut* of 10 ph.e.s (7 ph.e.s above pedestal) for both camera options, we found sets of supercuts, which we applied to the simulated spectra. After applying the shape and the orientation cuts for the three bins of the parameter MaxDIST, together with a cut in the asymmetry of images (to differentiate between *tail* and *head* of the image), we obtained the results shown in table 1 for the high QE HPMT camera and in table 2 for the classical PMT camera, respectively.

Table 1: The quality factor calculated for different MaxDIST bins, for the enhanced QE HPMT camera.

MaxDIST bin	Gamma Acceptance	Proton Acceptance	Q
0.4°– 0.5°	0.451	0.0077	5.14
0.5°– 0.9°	0.452	0.0049	6.47
0.9°– 1.1°	0.446	0.0012	12.84

One can see, that the imaging analysis provides in average a Q factor of ∼7–8 for MAGIC, which, in combination with the powerful pre-selection of gammas at the trigger level, provides

Table 2: The quality factor calculated for different MaxDIST bins, for the classical PMT camera.

MaxDIST bin	Gamma Acceptance	Proton Acceptance	Q
0.4°– 0.5°	0.560	0.0031	10.10
0.5°– 0.9°	0.512	0.0055	6.91
0.9°– 1.1°	0.470	0.0031	8.41

a very high sensitivity. For example, one can estimate that a source like *3C279* in its active phase can be measured on the level of 5σ in a few minutes if its spectrum extends well above $20\,GeV$. A 5σ signal from the Crab Nebula can be measured in about 1 minute. We estimate that a gamma source with a flux of $\sim 5{\cdot}10^{-11}\,ph\,cm^{-2}\,s^{-1}$ above $10\,GeV$ can be detected by MAGIC at a statistical significance level of 5σ in 100 hours of observation.

7.5. The Energy Resolution

The energy resolution for the MAGIC telescope has been determined for the set of given fixed energies, as well as for the entire spectrum above $10\,GeV$ from a simulated source with a spectral index $\alpha = -2.5$. In the derivation of the energy resolution of a telescope one should note that, for a given energy, the Cherenkov photon lateral distribution changes only slightly between some minimal radius of 50–60 m from the shower core and till the hump at about 125 m. For impact parameter range less than 50–60 m the images become progressively more round (which means a low efficiency for discrimination of gammas against hadrons) and also the fluctuations of the total measured charge from showers are larger. Beyond the hump there is a transition region where the photon density (read the measured charge) rapidly decreases and therefore showers of the same energy show up less and less charge. After the transition region one obtains again a reasonable resolution, but already with several times less total charge compared to the region before the hump. Therefore it is obvious that for the best energy reconstruction one has to avoid the transition region and select from the "measured" data only those showers which are in the above mentioned limits for the impact parameter. Preliminary results show that MAGIC will provide an average energy resolution of $\sim$ 35% above the threshold. This resolution is dominated by sub-$100\,GeV$ showers. However, this can result in a much better resolution for the higher energy part of the spectrum. For example, simulations show that MAGIC can yield an energy resolution better than $\sim$15% for energies above 250 GeV.

7.6. The Angular Resolution of the MAGIC Telescope

We investigated the angular resolution for the MAGIC telescope above a threshold of 10 GeV for the high QE HPMTs camera. We used the technique described in (Akerlof, 1991) to find the number of excess events from a point source in sky coordinates. For this purpose by using the Monte Carlo events we simulated a gamma source in the camera centre with the flux normalisation and the exponent given by the equation already mentioned in the paragraph 7.3. In fig. 8 we show the angular resolution for the MAGIC telescope above $10\,GeV$, which amounts to 0.2° (standard deviation of the 2-dimensional gaussian fit). Note that the angular resolution depends strongly on the energy. The fluctuations in showers decrease as the energy increases. Therefore, the angular resolution improves when one increases the lower cut on energy.

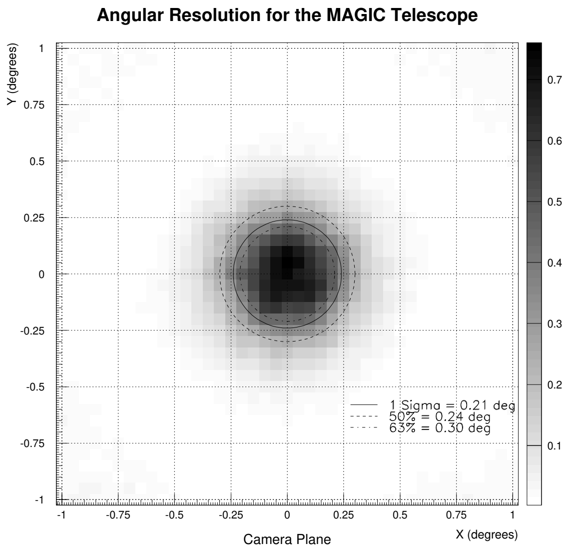

Fig. 8: The simulated angular resolution for MAGIC for a point source of gammas for energies $E \geq 10\,GeV$.

8. Conclusions

We have presented here the main results of Monte Carlo studies performed for the $17\,m$ diameter MAGIC telescope for both the high QE HPMT and the classical PMT camera options. For the classical PMT camera we calculated a threshold of $\sim 30\,GeV$ while for the HPMT camera a threshold of $\sim 8\,GeV$ is possible. The achievable Q factor in the conservative second moment analysis of images is in the range of 7–8, which, together with the high trigger efficiency in hardware for gammas and very low efficiency for protons, will provide a very high sensitivity for the telescope.

In the "satellite domain" of $E \leq 100\,GeV$, MAGIC will provide a 3–4 orders of magnitude higher rate from gamma sources than the satellite detectors. A Crab-like source can be detected at a signal level of 5σ in about 1 minute of observations. We believe MAGIC will play an important role in the rapid development of ground based gamma ray astronomy allowing us to "enter" the sub-100 GeV energy domain. It may serve as a prototype for future multi telescope gamma ray observatories.

9. Acknowledgements

We are indebted to many colleagues from the MAGIC design group for many critical discussions and useful suggestions. We acknowledge the partial support of the German Ministry of Education and Research BMBF, and the Spanish Research Council CICYT.

References

Akerlof, C.W, Cawley M.F., Fegan, D.J., et al., (1991) Astrophys. J., Lett. 337, L97.
Barrio J.A., et al., Design Report for the MAGIC telescope, in preparation.

Knapp J. and Heck D. (1995) Extensive Air Shower Simulation with CORSIKA: A User's Guide, Institut für Kernphysik, Forschungszentrum Karlsruhe GmbH.

Gaisser T. K. (1990) Cosmic Rays and Particle Physics, Cambridge University Press.

Mirzoyan R., Fernandez J., Lorenz E., Mueller N., Rauterberg G., Petry D., (1995) Proc. Int. Workshop "Towards The Major Atmospheric Cherenkov Detector-IV", ed. M. Cresti, Padova, Italy, pp. 230–240.

Mirzoyan R. and Lorenz E., (1994) preprint of Max-Planck-Institut für Physik, München, MPI-PhE/94-35.

Vacanti G., Fleury P., Jiang Y., et.al., Astroparticle Physics 2 (1994) pp. 1-11.

Weekes T.C. and Turver K.E., Proc. 12th ESLAB Symp., Frascati, Italy, 24-27 May, (1977) (ESA SP-124, July 1977).

Wiebel B 1994 Chemical composition in high energy cosmic rays, Fachbereich Physik Bergische Universität Gesamthochschule Wuppertal, WUB 94-08.